PARTICLE DISPERSION IN SUPERSONIC SHEAR LAYER BY DIRECT NUMERICAL SIMULATION

YANNICK BURY* and JEAN-LUC ESTIVALEZES
(estivale@onecert.fr)
ONERA DMAE, 2 Av Edouard Belin, BP 4025, 31055 TOULOUSE, FRANCE

Abstract. In experimental measurements like Laser Doppler Velocimetry, small solid or liquid particles are used to tag the flow in order to measure fluid velocity. In this case, particles are supposed to have the same behaviour as fluid particles in order to give reliablity to the experimental measure. However it has been shown [5] that noticeable errors can appear in the rms velocity measurement of supersonic jet or shear layer, even if care has been taken concerning particle seeding of the flow. The aim of this paper is to use direct numerical simulation of particle-gas flow to investigate this phenomenon.

1. INTRODUCTION

We are mainly concerned with three dimensional supersonic mixing layers. In such flows, beyond convective Mach number greater than 0.6, stability theory and direct numerical simulations show that oblique modes are much more rapidly amplified than two dimensional modes [11] (which correspond to the incompressible modes) leading to Λ vortices which are staggered in the streamwise direction. This particular behaviour could involve strong modification in mixing process. The object of the present work is to investigate how those highly three dimensional structures influence particles dispersion and the implications it can induce on velocity measurement by Laser Doppler Anenometry. Moreover, we will restrict ourselves in this study to the transitional stage of the mixing layer development as in the experiments of [5] discripancies on rms velocity have been observed only few diameters downstream of the jet outlet.

* now at Institut de Mécanique des Fluides de Toulouse, Av Camille Soula, 31400 TOULOUSE, FRANCE

P. R. Voke et al. (eds.), *Direct and Large-Eddy Simulation III*

2. NUMERICAL METHOD

2.1. GOVERNING EQUATIONS

The full time dependent Navier-Stokes equations for three-dimensional fluid motion are written in a non-dimensional conservative form. For a three-dimensional cartesian case, we have :

$$\frac{\partial U}{\partial t}+\frac{\partial F}{\partial x}+\frac{\partial G}{\partial y}+\frac{\partial H}{\partial z}-\frac{\partial F_v}{\partial x}-\frac{\partial G_v}{\partial y}-\frac{\partial H_v}{\partial z}=0 \tag{1}$$

U is the vector of conservative variables :

$$U=(\rho,\ \rho u,\ \rho v,\ \rho w,\ E)^T \tag{2}$$

F, G, H are the non-viscous fluxes. F_v, G_v, H_v are the viscous contributions. Here ρ, u, v, w, E denote respectively the density, fluid velocity components in the directions x, y and z, and the total energy (sum of the internal and kinetic energy). Non-dimensionalization of these equations is with respect to reference quantities, namely a reference length L^*, velocity U_1^*, density ρ_1^*, temperature T_1^*, and viscosity μ_1^*. L^*/U_1^* is the time reference scale, while $\rho_1^* U_1^{*2}$ is the pressure (and total energy) reference. The superscript * refers to a dimensional quantity. In our case, as we are interested by a temporal mixing layer, the reference length is chosen as the initial vorticity thickness of the longitudinal velocity profile : $L=\delta_{\omega 0}$, the reference velocity, temperature, density and viscosity are respectively U_1^*, T_1^*, ρ_1^*, μ_1^*, which are the far field values of the upper stream (cf 1). Using this non-dimensional scheme, we introduce the Reynolds number of the flow $Re=\rho_1^* U_1^* \delta_{\omega 0}/\mu_1^*$ and the Mach number which is in our case equal to the convective Mach number M_c is $M=U_1^*/\sqrt{\gamma \mathcal{R}^* T_1^*}$, where $\mathcal{R}^*=287.15\ J\ kg^{-1}\ K^{-1}$. The Prandtl number, assumed to be constant, is defined by $Pr=\mu^* C_p^*/k^*$ where k^* is the thermal conductivity. The viscosity follows Sutherland's law. The system is completed by the definition of the total energy, written in non-dimensional form as :

$$E=\frac{p}{\gamma-1}+\frac{1}{2}\rho(u^2+v^2+w^2) \tag{3}$$

and by the perfect gas law :

$$\frac{p}{\rho}=\frac{T}{\gamma M^2} \tag{4}$$

2.2. NUMERICAL SCHEME

Equations are solved using a finite volume high order extension of MacCormack's scheme due to Gottlieb and Turkel [4]. This scheme has already been used by

many authors for boundary layer simulations [1], [2], for mixing layer simulations [9], [10], [12], and for supersonic jet flow studies [7]. Based on predictor corrector phases, the scheme is explicit, second order accurate in time and fourth order in space. The time step Δt follows a CFL condition, and Fourier criteria. Extension to three dimensions and to the complete fluid motion equations is done through a directional splitting sequence :

$$\begin{aligned} U^{n+2} &= L_{zv}^{-}L_{yv}^{-}L_{xv}^{-}L_{z}^{-}L_{y}^{-}L_{x}^{-}L_{zv}^{+}L_{yv}^{+}L_{xv}^{+}L_{z}^{+}L_{y}^{+}L_{x}^{+}U^{n} \\ U^{n+4} &= L_{xv}^{+}L_{yv}^{+}L_{zv}^{+}L_{x}^{+}L_{y}^{+}L_{z}^{+}L_{xv}^{-}L_{yv}^{-}L_{zv}^{-}L_{x}^{-}L_{y}^{-}L_{z}^{-}U^{n+2} \end{aligned} \tag{5}$$

L_x, L_y, L_z, L_{xv}, L_{yv} and L_{zv} correspond respectively to the implementation of F, G, H, F_v, G_v and H_v. L_i^+ (with $i = x$, y, or z) refers to a sweep in the direction i with forward predictor and backward corrector. The alternate version L_i^-, employs a backward predictor and forward corrector.

2.3. BOUNDARY CONDITIONS AND INITIAL CONDITIONS

Because we deal with temporal mixing layer cf 1, periodic boundary conditions are used in the streamwise and spanwise directions (x and y directions). As we are considering an unbounded compressible mixing layer, non reflective boundary conditions based on Thompson work [13], [3] are used in the cross-stream direction (z direction).
Initialization of velocity, temperature and density fields consists of two parts, the mean profiles and the pertubations from linear stability theory [11]. The mean non dimensional velocity profile in the streamwise direction is :

$$\overline{u} = \tanh(2z) \tag{6}$$

The mean non dimensional temperature and density profiles are given by Crocco relations:

$$\begin{aligned} \overline{T} &= M_c^2 \frac{(\gamma-1)}{2}(1-\overline{u}^2)+1 \\ \overline{\rho} &= \frac{1}{\overline{T}} \end{aligned} \tag{7}$$

The initial disturbance field is specified by :

$$\begin{aligned} u' = \; & A_1 \mathrm{Real}\{\hat{u}(\alpha,0)e^{i(\alpha x+\phi)}\}+ \\ & A_2 \mathrm{Real}\{\hat{u}(\alpha,\beta)e^{i(\alpha x+\beta y)}+\hat{u}(\alpha,-\beta)e^{i(\alpha x-\beta y)}\} \end{aligned} \tag{8}$$

where $\hat{u}(\alpha,\beta)$ is an eigenfunction of the linear instability wave with streamwise wavelenght $L_x = 2\pi/\alpha = 13.36\,\delta_{\omega 0}$ and spanwise wavelenght $L_y = 2\pi/\beta = 13.36\,\delta_{\omega 0}$. It consists of a two dimensional and a pair of oblique waves. The angle of the oblique waves with the x direction is 45^o . Similar disturbances are added for ρ',

v', w', and T'. Here the value of the phase is $\pi/2$ in order to get the translative mode [11], [8].

2.4. PARTICLES DISPERSION SIMULATION

The following assumptions are made for the dispersed phase :

- dilute flow,
- all particles are rigid spheres,
- particle-particle interactions are neglected,
- density of particles is much larger than that of the fluid
- gravity is negligible.

With those assumptions the non dimensional particles motion equation writes:

$$\frac{d\vec{V}}{dt} = \frac{C_d}{St}(\vec{U} - \vec{V}) \qquad \frac{d\vec{X}}{dt} = \vec{V} \tag{9}$$

where $\vec{U}$ is the fluid velocity at the particle location and $\vec{V}$ is the particle velocity. $St = \rho_p^* d_p^{*2} U_1^* / 18\mu^* \delta_{\omega_0}$ is the Stokes number and C_d is the modified Stokes drag factor coefficient ($C_d = 1 + 0.15 Re_p^{0.687}$, for particle Reynolds number $Re_p = |\vec{U} - \vec{V}| d_p / \nu$ lesser than 1000). The velocity and particle position equations are integrated by the fourth order Runge-Kutta method. Fluid velocity at particles positions is interpolated by fourth order Hermite polynomials.

3. MESH DEPENDANCE STUDY FOR THE FLOW FIELD SIMULATIONS

Before dealing with particle flow simulations, we would like to check mesh dependance for the flow field simulation in order to determine the best compromise between computational cost and spatial resolution. To do that, we have run the flow solver with various resolutions. For the case considered in this paper, the numerical domain is a parallelipiped as described previously. We have used four different grids ranging from 32x32x32 to 96x96x96. In all thoses cases, the grids are regular rectangular ones in the three spatial directions, no particular stretching is used. The Reynolds number for the simulations is $Re = 400$, and the convective Mach number is $M_c = 0.8$. On the figure 2 a), we have drawn the evolution of the normalized vorticity thickness , $\delta/\delta_{\omega 0}$ in fonction of the non dimensional time $tU_1^*/\delta_{\omega 0}$. As can be seen on that figure, the curves corresponding to the 64x64x64 and 96x96x96 grid points are nearly similar. In order to emphasize the difference between the various grid resolutions, one dimensional kinetic energy spectrum in

the streamwise direction has been computed. To perform this Fourier analysis, first the two-dimensional kinectic energy spectrum in streamwise and spanwise direction and integrated in crosstream direction is evaluated by:

$$E(k_x,k_y,t) = \int_{-L_z/2}^{L_z/2} \hat{\mathbf{u}}(k_x,k_y,z,t)\hat{\mathbf{u}}^{\dagger}(k_x,k_y,z,t)dz \tag{10}$$

where $\hat{\mathbf{u}}^{\dagger}(k_x,k_y,z,t)$ is the complex conjugate of $\hat{\mathbf{u}}(k_x,k_y,z,t)$. The one-dimensional kinetic energy spectrum in the streamwise direction is defined by

$$\mathcal{E}(k_x,t) = \int_{k_y} E(k_x,k_y,t)dk_y \tag{11}$$

A similar definition is used to get the one dimensional kinetic energy spectrum in the spanwise direction On the figure 2 b) are shown the different spectrum for the different resolutions, good agreement is obtain for the 64x64x64 grid resolution compared to the 96x96x96 one. From thoses results, one can think that the 64x64x64 grid resolution can be a good compromise to perform the particle flow simulations.

4. RESULTS FOR PARTICLE DISPERSION

4.1. PARAMETERS OF THE FLOW SIMULATION

Coming from the previous results on the flow field simulation, we have chosen 64x64x64 grid cells, uniformly distributed in the three spatial direction The Reynolds number based on δ_0 is 400 and the convective Mach number is 0.8. Amplitudes of the disturbances are $A_1 = A_2 = 0.025$. Initially, 64x64x64 particles are seeded uniformly in the computational domain (one particle per cell) and particle velocity at the beginning of the calculation in each computational cell is the same as the fluid velocity in the cell. Dispersion of particles with Stokes numbers ranging from 0.1 to 1000 were simulated. Since there are periodic boundary conditions in the streamwise and spanwise directions, particles which move out of the box in these two directions from one side will be put back in the domain from the other side. Particles which move out the box in the cross-stream direction will not be recovered.

4.2. STOKES NUMBER DEPENDENCE OF PARTICLE DISPERSION

On figure 3 a) is summarized the evolution of the root mean square of particle number per cell over the whole field versus the Stokes number for different times. It is defined by

$$N_{rms} = (\sum_{i=1}^{N_c} N_i^2/N_c)^{1/2} \tag{12}$$

Here $N_c = 64\text{x}64\text{x}64$ and at time $t = 0$, $N_{rms} = 1$. This quantity is used to determine the overall concentration character of particles.
It is obvious that particles with Stokes numbers close to unity have larger N_{rms} value which is similar to the results of [6]. It should be noted that unlike incompressible flows simulations, here three dimensional Λ-shaped large scale structures strongly affect the dispersion even in the early stages of the mixing layer destabilization. Indeed, we don't observe two dimensional pairing as in the incompressible shear layer. This can be clearly seen on figure 3 b) where a perspective view of a pressure surface, that enclose a minimum of pressure (associated with strong rotation) is shown.
In order to examine the dispersion patterns for the different Stokes numbers, we have used the plane concept already defined in [6]. It corresponds to a thin slice with a thickness of a computational cell. Indeed, for the (x,z) plane at $y = L_y/2$, it means a thin slice with $L_y/2 < y < L_y/2 + \Delta y$, where Δy is the mesh spacing in the y direction.
We have drawn on figure 4 the distribution of the particles in the plane (x,z) at $y = L_y/2$ at time $t = 26$. For the smallest Stokes number, the particles seem to follow quite closely the fluid particles. Particles with Stokes number close to unity tend to accumulate around the edge of the three dimensional large scale structures. For larger Stokes numbers, the dispersion of particles in the cross-stream direction is decreasing, indeed the particles are less influenced by the Λ shaped vortices.
On figure 5, is drawn the particles distribution in the plane $z = 0$. The accumulation of the particle with Stokes number of unity on the edge of the vortex is clearly seen on that figure. Those particles trace the projection of the three dimensional coherent structures on that plane.
On figure 6, the particles distribution in the plane $x = L_x/2$ is plotted. Here again, the structure projection on this plane is obvious when one looks for $St = 1$ particles locations. Actually, theses particles seem to roll up around the arms of the Λ vortex in an helical way.
From this plane cut, particles with $St = 10$ show a quite different behaviour. Clearly, those particles are less sensitive to the vortex, and there is no such accumulation at the egde of the vortex arms, even if a void zone is present inside the vortex. For greater particle Stokes number, there is no more effect of the 3D vortex on the particle distribution, only a wavy movement can be seen on this plane cut.
In order to quantify the influence of those structures on particle dispersion the root mean square of particle number per cell for (y,z), (x,z), (x,y) planes, $N_{rms}(x)$, $N_{rms}(y)$, $N_{rms}(x)$ has been evaluated at time $t = 26$ (figures 7 a), b), c) for various Stokes numbers. For example $N_{rms}(x)$ is defined by :

$$N_{rms}(x) = \left(\sum_{i=1}^{N_{cp}} N_i^2(x)/N_{cp}\right)^{1/2} \tag{13}$$

where N_{cp} is the total number of computational cells in the plane (y, z) and $N_i(x)$ is the number of particles in the ith cell of that plane. The same definition is used for the two others quantities $N_{rms}(y)$ and $N_{rms}(z)$.
On figure 7 a), we can observe how the particles with different Stokes numbers concentrate along the streamwise direction. The maximum concentration is obtained for particles of unity Stokes number, when concentration is minimal for small and larger Stokes numbers. Moreover, the trend observed on that figure for the Stokes number which gives the maximum concentration, is completely opposite to that obtained for incompressible shear layer [6]. Even though for the incompressible case, $N_{rms}(x)$ is maximum at the boundaries of the computational box in x direction (for x near 0 and x near L_X) and minimal elsewhere, here $N_{rms}(x)$ is maximum in the center of the box (in x direction) and minimal at the boundaries. This emphasizes that dispersion mecanisms are really different in the two cases.
The next figure 7 b) gives the particles accumulation for the spanwise y direction. The same conclusions as in the previous figure can be drawn. The local minima observed for Stokes number of 1 show the trace of the arms of the Λ vortex whereas Stokes number of 10 particle present in that zone a local maxmium.
The figure 7 c) shows the particle accumulation in the cross-stream direction. Due to the lack of pairing of spanwise vortex, the maximum concentration for the different Stokes number is restricted to a zone of size $2\delta_0$ centered at $z = 0$. Maximum concentration is obtained with $St = 1$ particles. This is consistent with the fact that supersonic shear layer gives rate of growing much smaller than the incompressible one. From these three figures, the level of concentration in the three direction is much lower compared to the incompressible case. This shows that particle dispersion is our case much more threedimensional than in the incompressible case.

4.3. RESULTS OF PARTICLE DISPERSION FOR NON UNIFORM SEEDING

Whereas in the previous section, uniform seeding of particles has been used, i.e. one particle per cell for all the computational cells, here we would like to study the influence of non uniform particle seeding on the particle dispersion. Two cases have been considered. In the first one, only the upper half of the domain is seeded with one particle per cell; in the second one, the half lower of the domain is seeded in the same way. To compare the effect of non uniform seeding on the particle dispersion, we have calculated the components of the tensor of the particle velocity fluctuations. Mean values of particle velocities are calculated by plane averaging in the homogeneous directions, then particle velocity fluctuations are given by :

$$u' = u - \langle u \rangle$$

where u is the particle velocity in the direction x. From this, we can obtain for example $\langle u' v' \rangle$. This study on non uniform seeding has been done only for Stokes numbers 0.1 and 1. On the figure 8 and 9, we have plotted the various statistics versus the cross-stream direction for non uniform seeding (upper and lower) and for the two Stokes number, respectively, $St = 0.1$ and $St = 1$. The aberrant point on the $\langle u'^2 \rangle$ profile for the half upper seeding case at $St = 1$ is due to an under sampling in the average calculation. In fact for that particular plane, there are not enough particles to give a converged statistic. On the figure 10 are plotted the same quantities, but now for uniform seeding. The comparison of the three figures is self explainatory. For the two Stokes numbers, the profiles are shifted compare to uniform seeding. Moreover, the maximun values of the profiles are different in the two cases. This strong difference between the two type of seeding is crucial for the Laser Doppler Velocimetry application. Even, if seeding particles are small enough in order to closely follow fluid particles and so assumed to give a reliable experimental measure, non uniform seeding can completely alter the experimental measure.

5. CONCLUSION

Direct numerical simulations of particles dispersion in supersonic 3D mixing-layer have been carried out. First comparisons with the incompressible case show important differences due to strong three-dimensionality of such flows. Particles with Stokes number close to unity are centrifuged to the periphery of large scale vortices and give the maximum dispersion. Because of the Λ shape of those vortices and because no pairing of two-dimensional structure is present, dispersion behaviour is very different from the incompressible case. Non uniform seeding has been shown to have a great impact on fluctuating particles velocity leading to shifted profiles compared to uniform seeding. As a consequence, velocity measurements by Laser Doppler Velocimetry can be altered and not reliable.

References

1. Bayliss, A., P. Parikh, L. Maestrello, and E. Turkel: 1985, 'A Fourth-Order Scheme for the Unsteady Compressible Navier-Stokes Equations'. *AIAA Paper 85-1694.*
2. Ducros, F.: 1995, 'Simulations numériques directes et des grandes échelles de couches limites compressibles'. Ph.D. thesis, Institut National Polytechmique de Grenoble.
3. Gamet, L. and J. Estivalezes: 1995, 'Non-reflexive Boundary Conditions applied to Jet Aeroacoustics.'. *AIAA Paper 95-0159.*
4. Gottlieb, D. and E. Turkel: 1976, 'Dissipative Two-Four Methods for Time Dependent Problems'. *Mathematics of Computation* **30**, 703–723.
5. Jacquin, L., S. Mistral, P. Geffroy, and G. Losfeld: 1991, 'Etude d'un jet supersonique coaxial chauffé'. Technical report, ONERA.

6. Lin, W., J. Chung, T. Troutt, and C. Crowe: 1998, 'Direct numerical simulation of a three-dimensionnal temporal mixing layer with particle dispersion'. *J. Fluid Mech.* **358**, 61–85.
7. Mankbadi, R., M. Hayder, and L. Povinelli: 1993, 'The structure of supersonic jet flow and its radiated sound.'. *AIAA Paper 93-0549.*
8. Pierrhumbert, R. and S. Widnall: 1982, 'The two and three dimensional instabilities of a spatially perodic shear layer'. *J. Fluid Mech.* **144**, 59–62.
9. Ragab, S. and S. Sheen: 1991, 'Large-Eddy Simulation of a Mixing Layer'. *AIAA Paper 91-0233.*
10. Ragab, S., S. Sheen, and M. Sreedhar: 1992, 'An Investigation of Finite-Difference Methods for Large-Eddy Simulation of a Mixing Layer'. *AIAA Paper 92-0554.*
11. Sandham, N. and W. Reynolds: 1991, 'Three-dimensionnal simulations of larges eddies in the compressible mixing layer'. *J. Fluid Mech.* **224**, 133–158.
12. Tang, W., N. Komerath, and L. Sankar: 1989, 'Numerical Simulation of the Growth of Instabilities in Supersonic Free Shear Layers'. *AIAA Paper 89-0376.*
13. Thompson, K.: 1987, 'Time Dependent Boundary Conditions for Hyperbolic Systems I '. *Journal of Computational Physics* **68**, 1–24.

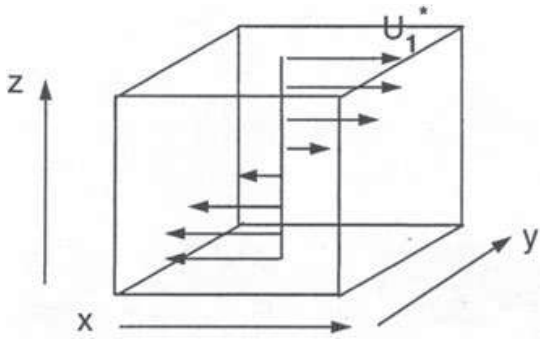

Figure 1. Temporal three dimensional mixing layer

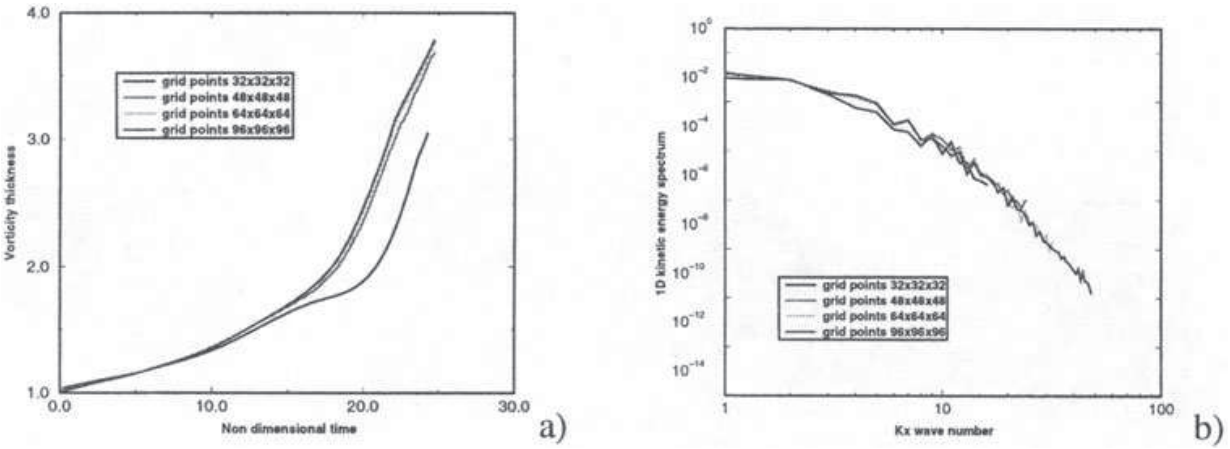

Figure 2. a) Evolution of the normalized vorticity thickness b) One dimensional kinetic energy spectrum at time $t = 26$

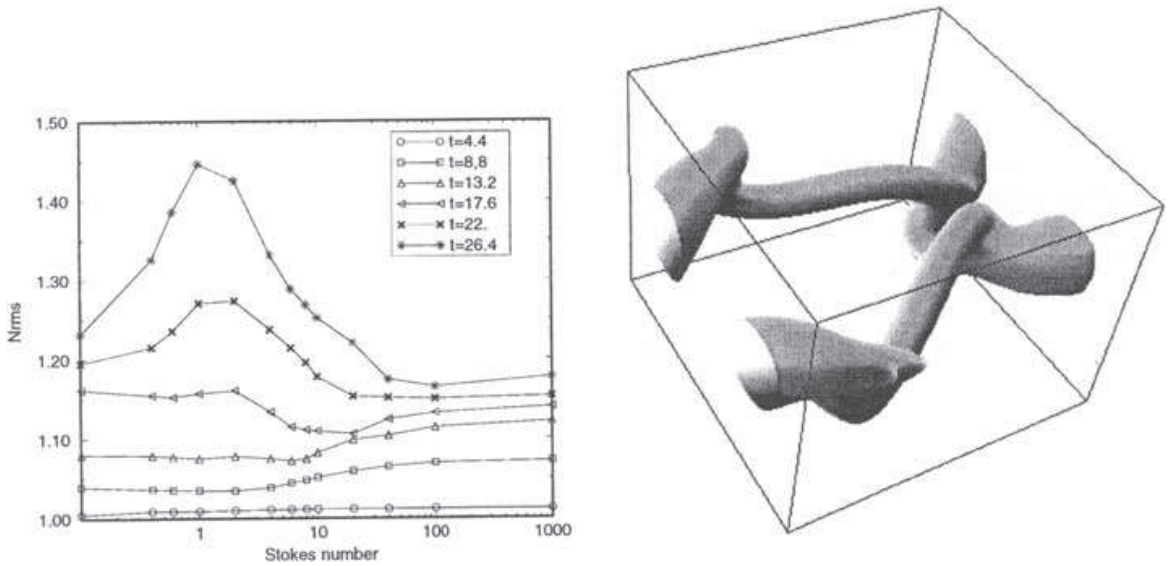

Figure 3. a) N_{rms} for different Stokes numbers b) isosurface of min pressure at time =20

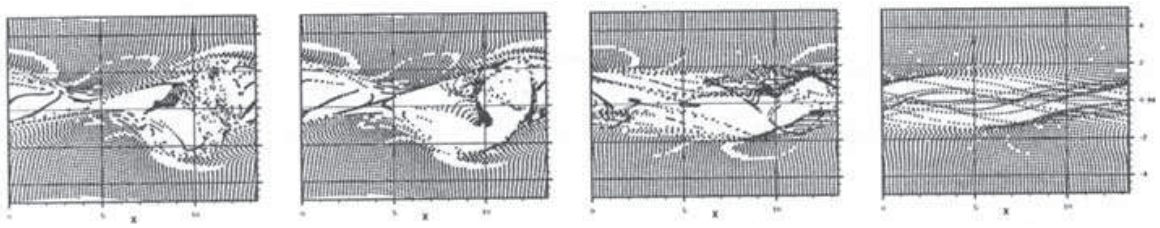

Figure 4. Plans cut of thickness Δy centered at $y = L_y/2$, from left to right $St = 0.1$, $St = 1$, $St = 10$, $St = 100$

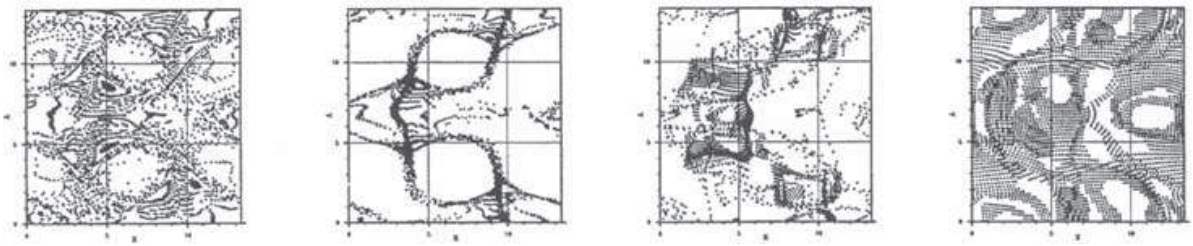

Figure 5. Plans cut of thickness Δz centered at $z = 0$

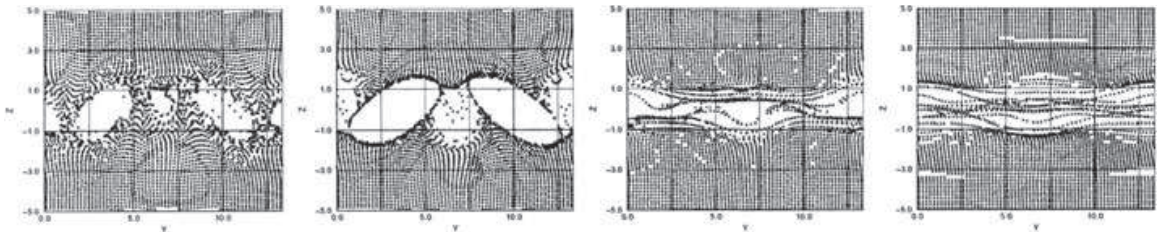

Figure 6. Plans cut of thickness Δx centered at $x = L_x/2$

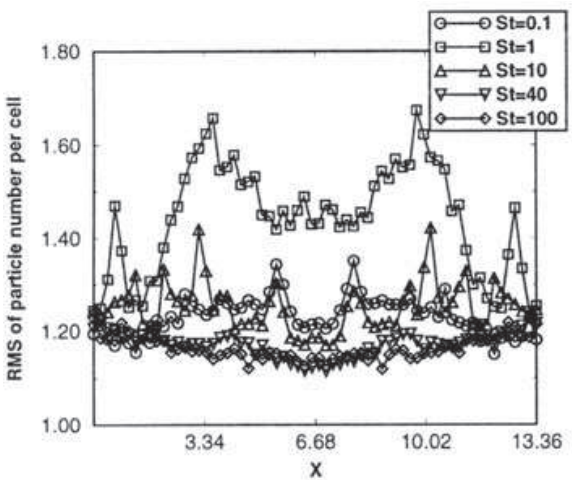

a) $N_{rms}(x)$ at time t=26

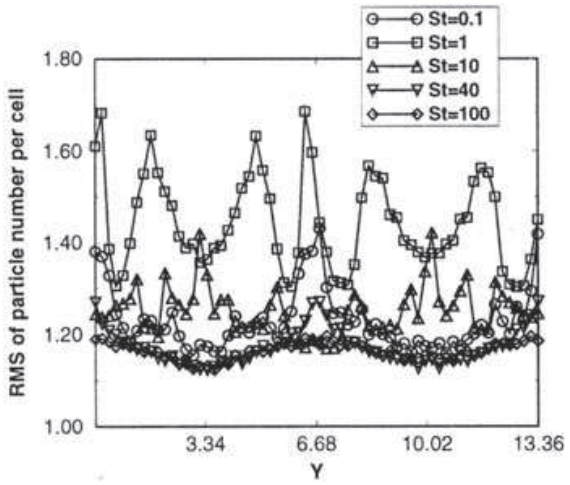

b) $N_{rms}(y)$ at time t=26

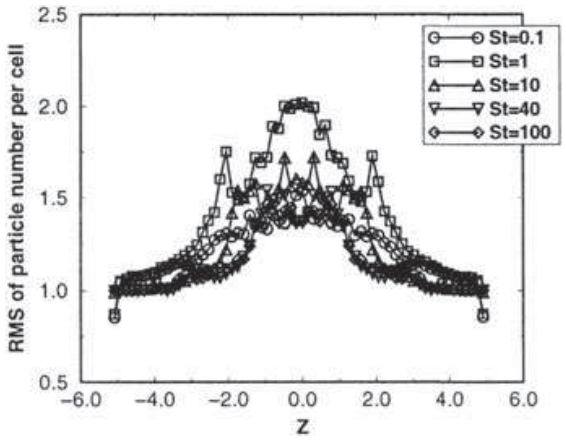

c) $N_{rms}(z)$ at time t=26

Figure 7. N_{rms} by direction at time t=26

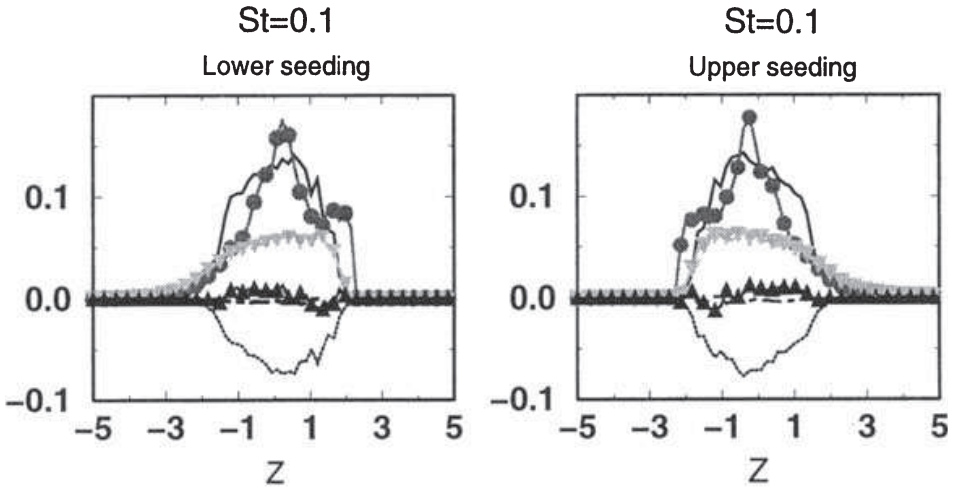

Figure 8. Non uniform seeding for St = 0.1

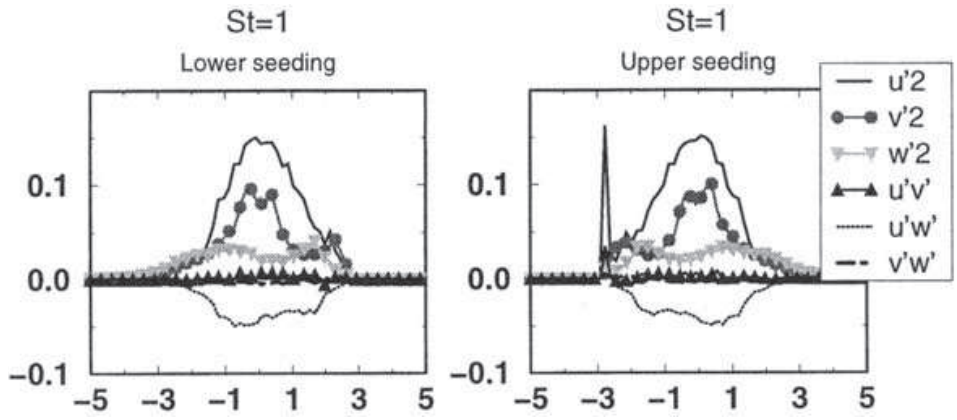

Figure 9. Non uniform seeding St = 1

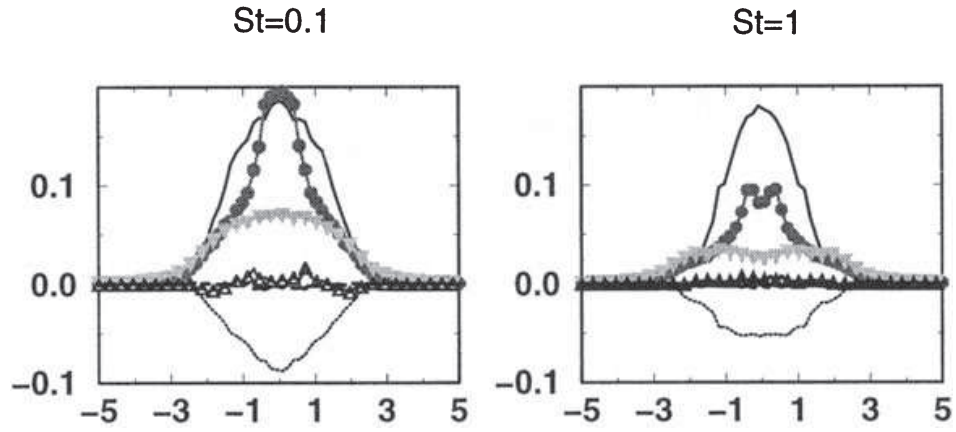

Figure 10. Uniform seeding